2860 *Biochemistry* **2010,** *49,* 2860–2868
DOI: 10.1021/bi901713r

BIOCHEMISTRY
including biophysical chemistry & molecular biology
Article

Molecular Dynamics Simulations of β-Ketoacyl-, β-Hydroxyacyl-, and *trans*-2-Enoyl-Acyl Carrier Proteins of *Escherichia coli*†

David I. Chan, D. Peter Tieleman, and Hans J. Vogel*

Biochemistry Research Group, Department of Biological Sciences, University of Calgary, Calgary, Alberta T2N 1N4, Canada

Received October 4, 2009; Revised Manuscript Received February 22, 2010

ABSTRACT: Acyl carrier protein (ACP) is the central player in fatty acid (FA) biosynthesis. It covalently binds all FA intermediates and presents them to the enzymes needed for elongation. Bacterial ACP must interact with a large number of proteins, which raises the question of how different acyl-ACPs are recognized and distinguished from each other. We performed molecular dynamics (MD) simulations of the FA synthase intermediates β-ketoacyl-, β-hydroxyacyl, and *trans*-2-enoyl-ACP spanning from 4 to 18 carbon groups in length. These forms of acyl-ACP have largely yet to be characterized experimentally, and our simulations provide a first insight into these structures. The simulations were conducted with the acyl chain directed into the solvent, as well as in a solvent-protected conformation inside the hydrophobic pocket of *Escherichia coli* ACP. Spontaneous migration from the solvent-exposed state into the hydrophobic binding pocket of ACP was seen in each of the intermediate classes studied, but not in all the individual simulations. This confirms that the intermediates can enter and utilize the same hydrophobic pockets as saturated acyl chains. In addition, a recurring, novel association of the acyl chains with loop I of ACP was observed that may be occupied transiently before entry into the hydrophobic pocket. The MD simulations of the acyl chains in a solvent-shielded state reveal that the polar functional group in the β position of the β-ketoacyl and β-hydroxyacyl chains anchors these moieties at the cavity entrance, while the chains without a polar group in the β position lack this additional anchoring atom. This leads to a binding mode in which the β-ketoacyl and β-hydroxyacyl chains are positioned further from the bottom of the pocket compared to the saturated and enoyl chains, particularly in short chain (< C12) ACPs. These observations suggest a rationale for how different acyl-ACP intermediates may be distinguished by FA synthase enzymes.

The fatty acid synthase (FAS)[1] system is an essential pathway that produces fatty acids (FAs) that are mostly used in the assembly of cell membranes (*1*, *2*). There are two types of FAS systems: type I systems that are found in humans and other eukaryotic organisms and type II systems, which are found in bacteria and eukaryotic plastids. The type I system is composed of long polypeptide chains that contain all the functions necessary for the formation of fatty acids, while the type II system expresses each of the enzymes as individual polypeptides. These major differences between the bacterial and human systems have made it an attractive system for the discovery of novel antibiotic targets and two are currently in use, triclosan and isoniazid (*3*, *4*). FA synthesis occurs in a cyclic process involving four key reactions that are necessary for the elongation of the fatty acyl chains. Initially, the acyl chain is extended by two carbon units by β-ketoacyl synthase, which adds a malonyl group to yield a β-ketoacyl chain. The second reaction is catalyzed by a β-ketoacyl reductase, reducing the acyl chain to a β-hydroxyacyl group. This is then converted to a *trans*-2-enoyl chain by β-hydroxyacyl dehydrase, which is reduced once more to complete the elongation cycle by an enoyl reductase (Figure 1). Each of the cycle intermediates is covalently bound to an acyl carrier protein (ACP) via a thioester bond to a phosphopantetheine linker that is attached at a conserved serine residue by ACP synthase (Figure 1). In bacteria, ACP is a 9 kDa, anionic protein that forms a globular protein with four α-helices, three of which run largely parallel to each other (*5*). These three helices form a hydrophobic pocket that houses saturated acyl chains bound to ACP and shields them from the solvent (*6*−*8*). The FAS system produces acyl chains up to 18 carbons in length by elongating chains containing as few as four carbons by two carbon units. Therefore, ACP binds a large number of different acyl chains and their corresponding β-ketoacyl, β-hydroxyacyl, and *trans*-2-enoyl intermediates. The acyl chains produced by ACP are utilized primarily for membrane biosynthesis but also for a number of other processes, such as lipid A synthesis, quorum sensing, and bioluminescence (*9*−*11*). Consequently, bacterial ACP must be able to interact with a large number of enzyme partners (*12*).

There are currently two hypotheses on how partner enzymes recognize ACPs that carry an appropriate substrate in their binding pocket. One scenario suggests that the enzymes participate in a trial and error process, in which they extrude the acyl chain from the hydrophobic pocket of ACP and thereby determine which substrate is present. Alternatively, ACP could undergo slight conformational changes based on which substrate is bound, which would then be recognized by partner enzymes and the acyl chain would only be extracted if the appropriate

†This work was supported by operating grants from the Canadian Institute of Health Research (CIHR) to H.J.V. D.P.T. is a CIHR New Investigator. D.P.T. and H.J.V. hold Senior Scholar and Scientist awards, respectively, from the Alberta Heritage Foundation for Medical Research.

*To whom correspondence should be addressed. Address: 2500 University Drive NW, Calgary, Alberta, Canada T2N 1N4. Tel: (403) 220-6006. Fax: (403) 289-9311. E-mail: vogel@ucalgary.ca.

[1]Abbreviations: ACP, acyl carrier protein; FA, fatty acid; FAS, fatty acid synthase; MD, molecular dynamics; PKS, polyketide synthase; SASA, solvent accessible surface area; SD, standard deviation.

 Published on Web 02/24/2010

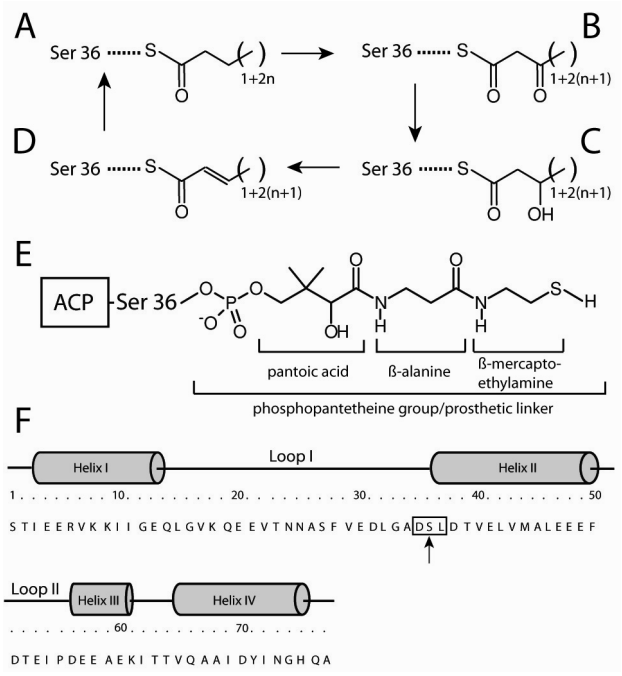

FIGURE 1: Schematic of the elongation cycle of fatty acid biosynthesis, showing the elongation intermediates simulated in this study. The saturated group (A) is extended by 2-carbon units through a condensation with a malonyl group to form a β-ketoacyl-ACP intermediate (B). This is reduced to yield a β-hydroxyacyl-ACP intermediate (C), which is dehydrated to form *trans*-2-enoyl-ACP (D). The cycle is completed via another reduction reaction to return to the saturated form, which is now extended by two carbon units (i.e., now $n = 1$). (E) The phosphopantetheine linker group attached to Ser36 of *Escherichia coli* ACP that is used to bind all of the intermediates via a thioester bond to its terminal sulfhydryl group. With the acyl chain bound, this may be referred to as the "arm". (F) Primary structure of *E. coli* ACP aligned with a secondary structure profile. Ser36 is pointed out with an arrow in the conserved DSL motif (box).

substrate is present (*13*). Although ACP structural information has been available for two decades and two ACP:enzyme complexes have been characterized by X-ray crystallography, it is still unclear how different acyl-ACPs are distinguished (*14*−*16*). In particular, there are no detailed structural data on how ACP is affected when bound to β-ketoacyl, β-hydroxyacyl, and *trans*-2-enoyl acyl chain intermediates. Such knowledge would aid in the understanding of ACP:enzyme interactions since it might help determine how ACPs carrying the appropriate substrate are recognized. To this end, we have conducted molecular dynamics (MD) simulations to study the effect of acyl-chain intermediates on the conformation of *Escherichia coli* ACP. We performed a comprehensive set of simulations consisting of ACP bound to each of the intermediates in the acyl chain elongation cycle ranging from 4 to 18 carbon groups in length. These simulations build on our previous MD studies conducted with saturated forms of acyl-ACP that are in excellent agreement with experimental data (*17*). Furthermore, in our previous study we made the observation that there is a second internal binding pocket for the fatty acids inside ACP, which was subsequently experimentally verified (*18*, *19*). This lays the foundation for the present study, in which we investigate acyl-ACP forms not yet characterized by, and not readily accessible to, conventional experimental methods.

EXPERIMENTAL PROCEDURES

Simulation Setup. MD simulations were set up for *E. coli* ACP containing the phosphopantetheine group and either a β-ketoacyl-, β-hydroxyacyl, or *trans*-2-enoyl fatty acyl chain in a solvent-exposed or a solvent-shielded conformation. The coordinates of ACP containing solvent-exposed attachments were all based on the crystal structure of *E. coli* butyryl-ACP (PDBID 1L0I (*6*)) analogously to ref *17*. ACP containing the acyl chains inside the hydrophobic pocket were based on either *E. coli* butyryl-, hexanoyl-, heptanoyl-, or decanoyl-ACP (PDBIDs 1L0I, 2FAC, 2FAD, 2FAE, respectively), depending on the acyl chain length simulated (*7*). The acyl chains were attached via the prosthetic linker and ranged in length from C4 to C18, increasing by two carbon units for each intermediate type. The parameters for the phosphopantetheine topology were taken from ref *17*, while the topologies for the elongation cycle intermediates were predominantly based on building blocks already parametrized in GROMOS96 43a2 (*20*). The parameters past the trans double bond were taken from ref *21* and the S-Cα-Cβ-Cγ dihedral was taken from ref *22*. The GROMOS96 forcefield parameters around the β-hydroxyl and β-ketone groups were derived from analogy to other segments from (*20*, *21*, *23*). For example, bond, angle, dihedral, charge, and atom types for the β-hydroxyl group were derived from similarity to threonine.

These 48 starting structures were placed in a dodecahedral box filled with approximately 14 000 or 12 000 explicit simple point charge water molecules depending on whether or not the acyl chain was solvent-exposed or buried, respectively. All the simulations were performed using the GROMACS 3.3.3 MD package (*24*, *25*) and the GROMOS96 43a2 force field containing improved alkane dihedral parameters (*20*). Virtual sites were used for nonpolar hydrogens, permitting the use of a longer, 5 fs time step (*26*). Using a longer time step provides more efficient sampling compared to the more common 2 fs time step, and it has been shown in separate studies (*26*, *27*) and in our test suite (see the Supporting Information) that the quality of the simulation is not affected by this alteration. After energy minimization and initial water equilibration, a total of 39 Na^+ and 24 Cl^- ions were added to the simulations of ACP with a solvent shielded acyl chain, while 46 Na^+ and 31 Cl^- ions were added to the simulations with a solvent exposed acyl chain. The difference is due to the slightly larger box that was used in the latter simulations. These ion numbers yield average salt concentrations of 150 mM, reflecting physiological conditions, and an overall neutral charge for the simulation box. The protein was equilibrated over 250 ps while lowering the position restraints in five distinct steps from 1000 to 0 kJ/mol nm^2. Production runs were conducted in triplicate for each starting conformation using different, randomly generated velocities to generate new sets of trajectories. This means in total, 3 FAS cycle intermediates were simulated for each of 8 chain lengths and in triplicate, adding up to 72 trajectories of the solvent-shielded acyl chains and an equal number of solvent-exposed acyl chains attached to ACP. Each production run was 20 ns in length, which is capable of capturing vibrational and fast loop motions, overall tumbling, as well as side chain rotations and reorientations. Importantly, dynamics, including association and dissociation events, of covalently bound ligands, such as the acyl chains studied here, can also be captured during this simulation period. On the other hand, protein folding and unfolding, large domain rearrangements, and noncovalent ligand binding are unlikely to be captured on this time scale. For detailed simulation procedures and parameters, see the Supporting Information. The analysis was conducted using various GROMACS analysis programs and VMD, which was also used to generate the structural figures of

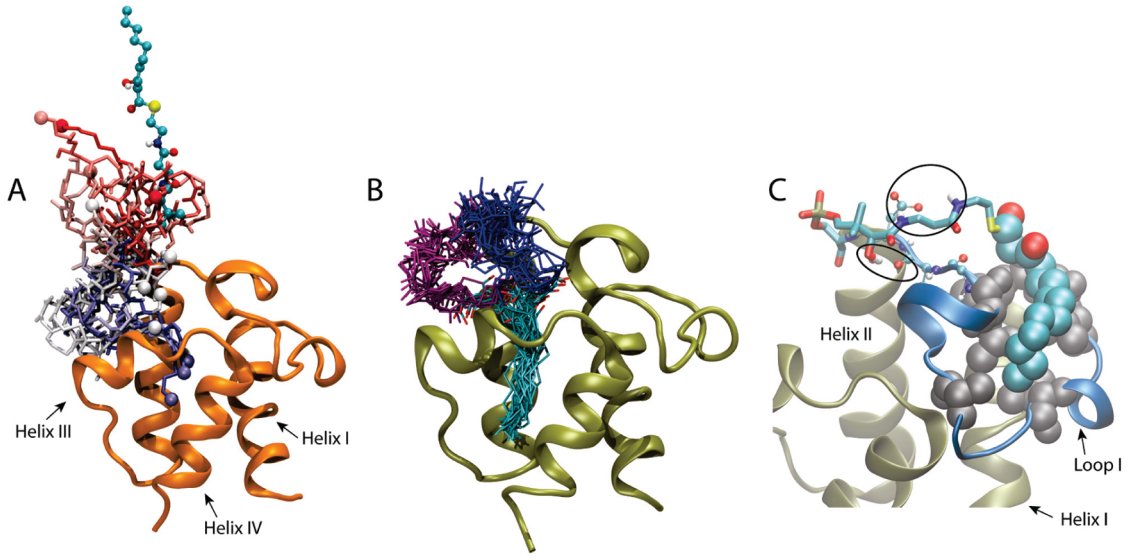

FIGURE 2: (A) Snapshots taken every 1 ns of the β-hydroxydecanoyl-ACP intermediate beginning with its acyl chain completely solvent-exposed moving into the hydrophobic binding pocket. The acyl chain is colored by atom type in its starting conformation directed straight up from the protein and subsequently in a continuous spectrum from red to blue as it moves into the hydrophobic pocket. The tips of the acyl chains are shown as spheres for clarity. (B) Snapshots taken every 0.5 ns of β-ketotetradecanoyl-ACP highlighting the two prominent linker positions (purple and blue) around which the linker fluctuates heavily. The acyl chain is shown in cyan. (C) Representative structure highlighting the association between the acyl group and loop I as described in the text. The acyl chain of the β-ketotetradecanoyl group shown here rests in a group of hydrophobic residues (gray spheres) in loop I (blue). At the other end of the arm, the prosthetic linker (stick representation) is stabilized by forming hydrogen bonds to the side-chain of Asp35 (large oval) and the carbonyl of Ala34 (small oval).

ACP (*28*). In addition, to investigate whether the specific parameters used in our simulation setup have an effect on their outcome, a test suite of simulations were performed with a 2 fs time step, the GROMOS96 53a6 forcefield (*29*), or charges solely derived from ProDrg (*30*). These results are shown in the Supporting Information (Table S1, Figure S1).

RESULTS

Acyl-ACP Simulations with Solvent-Exposed Acyl Chains. MD simulations of the acyl-ACP intermediates were set up in a solvent-exposed conformation in order to elucidate their binding mode, since there are currently no structural data available for these intermediates. Out of the 72 total solvent-exposed trajectories, 12 displayed a transition from the solvent-exposed starting conformation into the hydrophobic binding pocket of ACP in the center of the helix bundle (Table S2, Supporting Information). Each of the β-ketoacyl-, β-hydroxyacyl-, and *trans*-2-enoyl-ACP classes showed a transition into the pocket and sampled both sub pockets I and II, confirming that the intermediates use the same binding cavity as the saturated acyl chains (Table S2, Supporting Information). Similar to the saturated acyl-ACP simulations (*17*), the arm initially tumbles in various directions in the solvent and enters the binding pocket with the tip of the acyl chain first, followed by rapid penetration to the bottom of the cavity (Figure 2A). Once the acyl chain has moved into the hydrophobic binding pocket, it remains there for the remainder of the simulation and does not exit the pocket again. After acyl chain insertion, the prosthetic linker either fluctuates over the cavity opening or bends to the side between helices II and III and remains highly flexible (Figure 2B). This is also seen in the solvent shielded simulations.

In all of the simulations, ACP only displays minimal structural changes between the acyl bound and unbound forms, with the backbone RMSDs undergoing negligible changes with acyl chain insertion. Despite the overall stability of the ACP structure

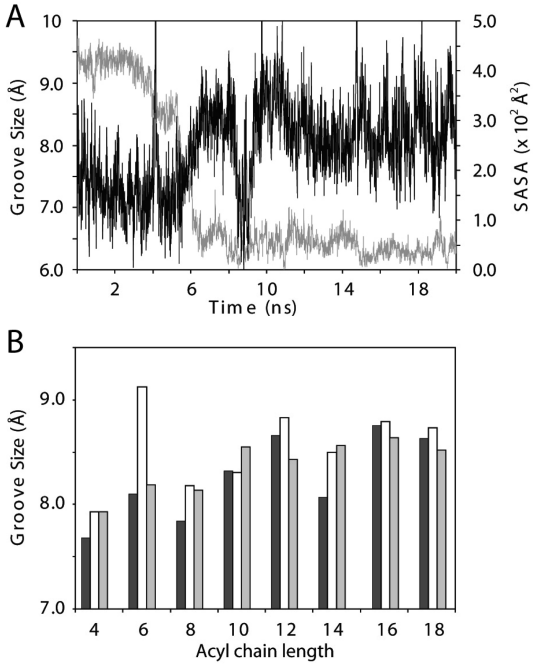

FIGURE 3: Changes in binding groove size (measured between Thr39 and Ala59) correlated with acyl chain insertion. (A) The size of the groove increases (black line) in concert with the transition of the acyl chain (β-ketohexadecanoyl-ACP shown here) into the hydrophobic binding pocket of ACP as indicated by the decreasing SASA of the acyl chain (gray line). (B) The size of the groove increases with the size of the acyl chain bound inside the hydrophobic binding pocket of ACP up to 12 carbon groups. Groove sizes of ACP bound to β-ketoacyl, β-hydroxyacyl, and *trans*-2-enoyl intermediates are shown in dark gray, white, and light gray, respectively.

during the acyl chain insertion process, the size of the groove opening between helices II and III increases going from the solvent-exposed to the solvent-shielded state. The pocket opens up slightly after acyl chain insertion, and in particular the

opening to the cavity becomes wider compared to when the acyl chain is solvent-exposed (Figure 3A). This can be quantified looking at the distance between the carbonyl carbons of Thr39 and Ala59 in helices II and III, respectively, on opposite sides of the groove (Figure 3). With the acyl chain in a solvent-exposed state, the groove averages 7.4 ± 0.5 Å and increases to 8.4 ± 0.5 Å upon acyl chain binding inside the hydrophobic pocket. This is analogous to what was observed in recently reported holo- and butyryl-ACP NMR structures, although the groove in those cases is noticeably larger, measuring 8.3 and 10.6 Å, respectively (*31*). The groove width in our simulations is also dependent on the acyl chain length bound inside the hydrophobic binding pocket, with the groove size (distance between Thr39 and Ala59) increasing from C4 to C12 intermediates and then leveling off (Figure 3B). The *E. coli* acyl-ACP crystal structures display a similar groove size at 8.4 Å; however, an increase in groove size with acyl chain length is not seen (*6*, *7*). Unlike the NMR structures (*31*), the N-terminal residues of helix III did not bend away from the protein core in the simulations but remained at a constant distance from helix II. Measured between carbonyl groups of Thr39 and Asp56 in helix II and the N-terminal end of helix III, respectively, the distance with the acyl chain bound was 10.7 ± 0.6 Å compared to 10.3 ± 0.9 Å with the chain removed from the pocket in the simulations. These distances compare very well with those observed in the acyl-ACP crystal structures, which average 10.4 Å, while the butyryl-ACP NMR structure measures 13.3 Å over the same distance (*6*, *7*).

Many of the trajectories in which the acyl chain did not traverse into the hydrophobic binding pocket from its solvent-exposed starting conformation displayed a recurring association with loop I of ACP (Table S2, Supporting Information). This interaction was observed in 28 out of the 72 total trajectories and was seen in each of the β-ketoacyl-, β-hydroxyacyl, and *trans*-2-enoyl intermediate types (Table S2, Supporting Information). Furthermore, in the MD simulations of saturated acyl-ACPs, this association is seen as well in the C10 and C12 forms of acyl-ACP (*17*). The most common hydrogen bonding interactions are between the side-chain carboxyl group of Asp35 and the backbone carbonyl of Ala34 to the pantoic acid hydroxyl and the β-alanine amide group on the prosthetic linker (Figure 2C). Additionally, the amide group in the β-mercaptoethylamine region formed hydrogen bonds to the groups in loop I mentioned above, as well as to the carbonyl groups of Val29 and Gly33. While the phosphopantetheine linker is involved in these hydrogen bonds, the acyl chain itself is frequently nestled into the groove formed by residues 15−33 of loop I (Figure 2C). This loop contains a number of hydrophobic residues, namely, Leu15, Val17, Val22, Ala26, and Leu32. In this surface groove, the acyl chain may rest for extended periods of the trajectory (e.g., > 10 ns). However, unlike entry into the hydrophobic binding pocket, the interactions with loop I are more readily reversible, as the acyl chain was observed to detach from loop I and adopt alternate conformations in certain trajectories. This is perhaps not surprising, considering that the solvent accessible surface area (SASA) of the acyl chain associated with loop I is much higher than when it is buried inside the hydrophobic binding pocket. For example, for the *trans*-2-octadecenoyl chain, the SASA is 290 Å^2 when associated with loop I, compared to 72 Å^2 when hidden in the hydrophobic binding pocket.

Solvent-Shielded Acyl-ACP Intermediates. The simulations of ACP containing solvent-shielded intermediates were set up with the attachments in the same binding pocket as the saturated acyl chains in the center of the three helix bundle. The results of the acyl-ACP intermediates simulations in the solvent-exposed conformation support the notion that these acyl groups are housed in this same hydrophobic binding pocket (vide supra). The backbone RMSDs were stable in most trajectories around 1.5−2.5 Å, and other than a slight unwinding of the C-terminus in a small proportion of the simulations, there were no major disruptions to the native ACP conformation. The acyl intermediates are buried to a different extent depending on the type of intermediate bound. The *trans*-2-enoyl chains are buried deeper into the hydrophobic pocket than the β-ketoacyl- and β-hydroxyacyl-chains of equal length as shown by the distance between the thioester oxygen and the bottom of the cavities (Table 1). This distance is consistently higher for the β-ketoacyl- and β-hydroxyacyl-intermediates compared to the *trans*-2-enoyl-intermediates in the short chain structures (< C12). In addition, for the short chain acyl groups (< C12), the thioester linkages in the keto- and hydroxyl-chains are further from the bottom of the cavity compared to their saturated counterparts, indicating that the saturated acyl chains are buried further inside the pocket (Table 1). The hexanoyl chains are the exception to this pattern because they are found in an alternate binding mode in the crystal structure (see Discussion) (*7*).

Table 1: Distance between Acyl Chain Thioester Oxygen and the Bottom of the ACP Pocket

chain length	β-keto chains	β-hydroxyl chains	*trans*-2-enoyl chains	saturated chains[a]
		(Å) ± SD		
4	13.5 ± 0.5	12.8 ± 2.9	11.9 ± 1.3	11.6
6	10.9 ± 2.1	10.1 ± 0.8	11.4 ± 1.8	12.3
8	14.4 ± 0.7	15.5 ± 0.5	14.0 ± 0.5	12.4
10	14.9 ± 0.7	14.7 ± 1.0	13.1 ± 0.7	13.9
12	14.8 ± 0.8	15.8 ± 1.4	14.7 ± 0.6	16.8
14	15.7 ± 0.8	16.8 ± 0.6	15.4 ± 0.5	19.0
16	15.8 ± 1.4	17.1 ± 0.8	17.2 ± 1.9	16.8
18	18.7 ± 0.8	18.0 ± 1.5	16.2 ± 1.8	17.7

[a]From data in ref *17* − no SD available.

The polar nature of the β-ketone and β-hydroxyl groups appears to be the driving force that draws these intermediates further out of the pocket compared to the saturated and enoyl acyl chains. The simulations show that the additional polar group preferentially rests at the cavity entrance rather than inside the cavity where there is a lack of hydrogen bonding partners (Figure 4). Averaged over all the β-hydroxyacyl-ACP simulations, the β-hydroxyl group forms ~0.5 hydrogen bonds with the protein. It preferably interacts with the carbonyl groups of Ile62 and Ala59, although a number of other, minor interactions are observed as well. The β-ketone group participates in hydrogen bonding with the protein as well, but to a far lesser extent (< 0.1 hydrogen bonds on average) because there are almost no hydrogen bond donors at the entrance to the hydrophobic binding pocket. The β-hydroxyl and β-ketone groups also heavily hydrogen bond with the solvent, averaging 0.81 and 0.35 hydrogen bonds, respectively. This is reflected in the SASA of the β-carbon and its attached oxygen or hydroxyl species, which is ≥5% in each of the β-hydroxyacyl- and β-ketoacyl-chains, independent of chain length (Table 2). The SASA of the two *trans*-enoyl double bond carbons, on the other hand, are shielded inside the

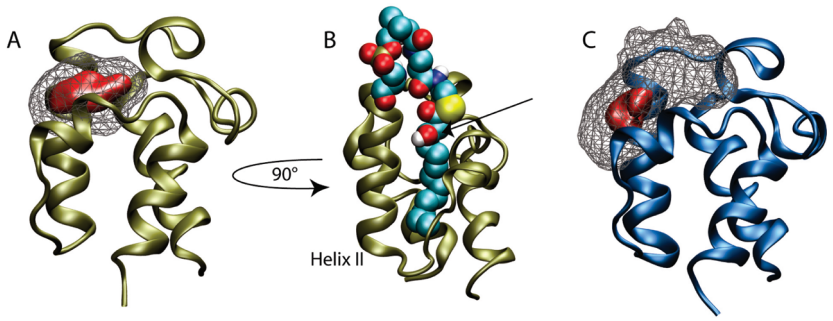

FIGURE 4: Preferred sites of the β-ketone and β-hydroxyl functional groups. (A) and (B) display β-hydroxytetradecanoyl-ACP, while (C) shows β-ketooctadecanoyl-ACP. The inner, red surface plot (A, C) represents the preferred location of the β functional group (fractional occupancy = 0.07), while the outer wireframe illustrates the conformational space sampled by the oxygen atom (fractional occupancy = 0.0005). (B) shows a snapshot of the trajectory in (A) rotated as indicated, with the prosthetic linker and its attached β-hydroxyacyl chain shown as spheres. This orientation demonstrates how the β-hydroxyl group (arrow) can penetrate into the solvent between helices II and III, where it may be recognized by enzymes of the FAS system.

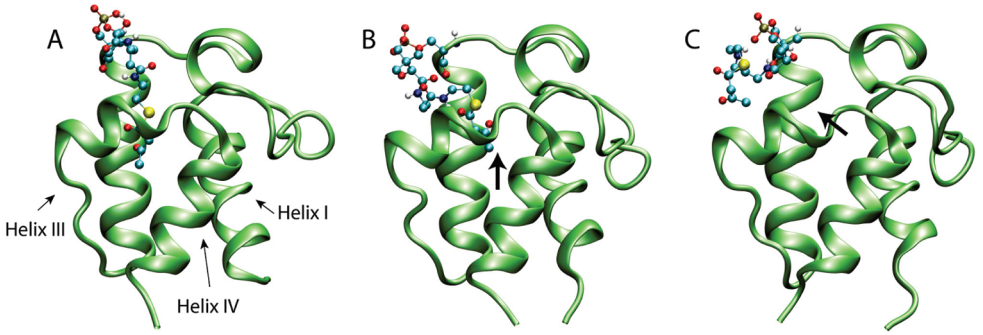

FIGURE 5: Spontaneous acyl chain extrusion process. (A) The β-ketobutyryl chain starts off deeply buried in the hydrophobic binding pocket of ACP which is raised out of the pocket slightly as the β-keto group has a propensity to rest at the cavity entrance due to its polar character (B). (C) Continued fluctuations of the arm eventually cause the acyl chain to slip out of the cavity and tumble in solution. This pathway is similar to the reverse of the acyl chain entry process.

hydrophobic pocket during the simulations, particularly in the short-chain groups (Table 2). Since the enoyl group cannot participate in hydrogen bond formation, there is no enthalpic penalty when it is hidden inside the hydrophobic pocket.

In contrast to the saturated acyl-ACP simulations, in which none of the buried acyl chains exited the binding pocket (*17*), the β-ketobutyryl- and β-hydroxybutyryl-groups showed the extrusion of the prosthetic group from the hydrophobic pocket (Table S3, Supporting Information). These intermediates have the fewest hydrophobic groups, since two out of the four carbon moieties have attached oxygen atoms. Therefore, the only readily exposed carbon groups are a methylene immediately following the thioester bond and a methyl group at the tip of the acyl chain. This amount of hydrophobic character is apparently not sufficient to retain the acyl chain in the hydrophobic binding pocket where it was originally placed at the start of the simulation. In four out of six simulations, these groups exit the cavity for at least short periods of time. The exit pathway for these acyl chains is very similar to the mode of entry (Figure 5). The tip of the acyl chain samples various positions inside the binding pocket and at times comes close to the cavity entrance. The β-ketone or β-hydroxyl groups prefer being at the cavity entrance, as mentioned above, which also draws the tip of the acyl chain toward the cavity opening (Figure 5B). The tip then periodically slips out of the pocket and is directed into the solvent, but can also exit the cavity for longer periods of time (~6 ns). During this process, the structure of ACP does not undergo any major conformational changes. All the helices remain intact, and no major shifts in any of the structural elements are observed. The availability of

Table 2: Averaged Solvent Accessible Surface Area of Each Functional Group in Solvent Shielded Acyl-ACP Simulations

	β-keto group[a]		β-hydroxyl group[b]		*trans*-2-enoyl group[c]	
chain length	(Å^2)	%[d]	(Å^2)	%[d]	(Å^2)	%[d]
4	1.74	5.0	3.54	8.9	0.60	1.0
6	0.46	1.3	3.78	9.5	0.79	1.3
8	2.15	6.2	6.91	17.3	1.15	1.8
10	2.32	6.6	2.54	6.3	1.06	1.7
12	3.10	8.9	8.27	20.7	3.27	5.2
14	4.30	12.3	6.75	16.9	5.13	8.2
16	3.76	10.8	8.05	20.1	8.33	13.2
18	8.51	24.3	13.2	33.1	3.80	6.0

[a]SASA was calculated for the β-carbon and attached oxygen atom only. [b]SASA was calculated for the β-carbon and attached hydroxyl group only. [c]SASA was calculated for the β- and γ-carbons involved in the double bond. [d]% exposed is in relation to the SASA of these atoms in a fully solvent exposed acyl chain.

numerous hydrogen bonding partners for the prosthetic group appears to be important in the flexibility of the acyl chain. For example, in one of the β-hydroxybutyryl-ACP simulations, the β-hydroxyl group hydrogen bonds with the carbonyl group of Ile62 while the tip of the acyl chain rests in the binding pocket. When the acyl chain escapes the binding pocket, this hydrogen bond is broken and a new one forms between the β-alanine carbonyl group of the linker and the amide of Val29 (Figure 6). This specific hydrogen bonding example is not seen in all the trajectories, but a similar balance and network of hydrogen bonds for the prosthetic group is observed throughout all the simulations.

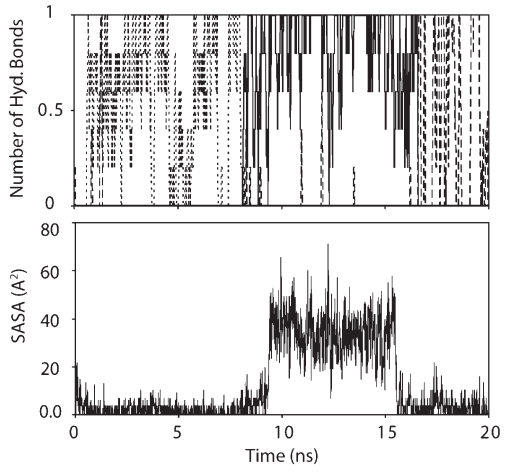

FIGURE 6: Phosphopantetheine group hydrogen bonding interactions. Hydrogen bonds between the prosthetic linker of β-ketobutyryl-ACP and the protein are shown during the acyl chain extraction and re-entry process (upper panel). The linker first forms hydrogen bonds with Ile62 (short dashes) that are broken upon acyl chain extrusion (which may be followed by the acyl chain SASA, lower panel), but are compensated for by new interactions with Val29 (black line). At about 16 ns, the acyl chain moves back into the hydrophobic pocket and the linker forms a new set of hydrogen bonds to Glu60 (long dashes). For plot clarity, hydrogen bond numbers were averaged over 50 ps.

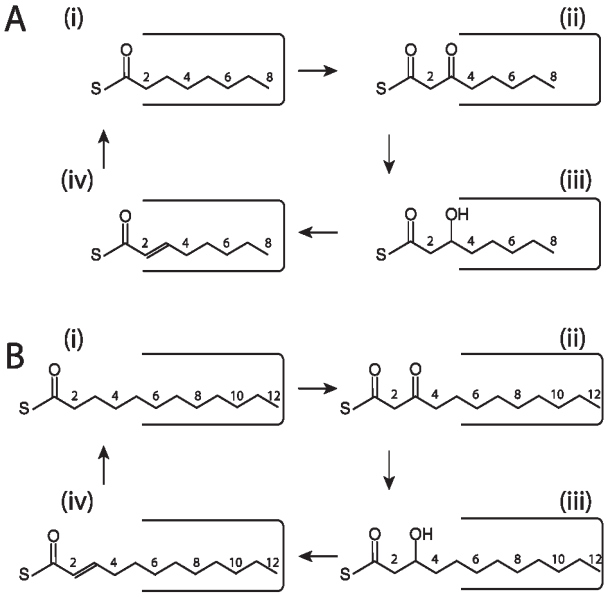

FIGURE 7: Schematic of the differences observed in the binding modes of (i) saturated-, (ii) β-ketoacyl-, (iii) β-hydroxyacyl-, and (iv) *trans*-2-enoyl-intermediates in short (A) and long (B) chain acyl groups. Short chain (≤C10) acyl-ACPs (A) shield the β-carbon in (i) and (iv), while in (ii) and (iii) the β-ketone and β-hydroxyl groups draw the chain out of the pocket further. In long chain (≥C12) acyl-ACPs (B), the β-position is solvent-exposed in each of the intermediates (i to iv) due to the large size of the acyl chains.

DISCUSSION

Acyl-ACP Intermediate Structures. ACP has long been the focus of much research and structural data for this protein became available over 20 years ago (*14*, *32*). Despite its extensive history, new insights regarding ACP structure and function continue to emerge (e.g., refs *33*−*35*). However, many areas such as enzyme:ACP interactions are still poorly understood. For example, there is currently no structural information on the acyl-ACP intermediates of the FA biosynthesis elongation cycle. Our MD simulations provide the first structural studies of the β-hydroxyacyl, β-ketoacyl, and *trans*-2-enoyl-ACPs. The binding mode of these chains is in part dictated by the type of intermediate that is attached to ACP. The additional polar group in the β-ketoacyl- and β-hydroxyacyl-intermediates makes it energetically less favorable for the chain to penetrate into the hydrophobic pocket as deeply as the nonsubstituted chains. In the saturated acyl chains, the thioester oxygen provides a polar anchor that hydrogen bonds with the solvent and the protein at the cavity entrance (*6*, *7*, *17*). In the β-ketoacyl and β-hydroxyacyl chains, the attachment of either group to the β-position provides a new anchor that determines the positioning of the acyl chain and prevents the prosthetic linker from being pulled into the hydrophobic cavity, especially in short chain (< C12) acyl-ACPs (Figure 7). The longer acyl chains (≥C12) are too large for the hydrophobic binding pocket, and consequently, the β-position is solvent-exposed as well in these structures (Figure 7B). Because of their increased length, the polar group does not draw the acyl chains out any further than the nonsubstituted, saturated equivalents (Table 1, Figure 7B). The enoyl chain on the other hand is similarly buried to the saturated chains, independent of acyl chain length (Figure 7).

The exceptions to this are the hexanoyl-chain simulations, which are deeply buried in the cavity in each of the three intermediate types. The published hexanoyl-ACP structure (PDBID 2FAC), that was used as the starting template for the C6 chains, features the linker in an alternate binding mode that lies 5 Å further inside the pocket compared to some of the other acyl-ACP structures (*6*, *7*). The hexanoyl intermediates do exit this binding mode in some instances, which is reflected in the larger standard deviations of the distances to the bottom of the pocket (Table 1), but the averages are still lower compared to the structures that adopt alternative binding modes. The second conformation is less frequently adopted, since only the two hexanoyl- and one heptanoyl-ACP display this binding mode, while the other *E. coli* and spinach acyl-ACP structures bind the protein differently (*6*−*8*).

Acyl-Chain Entry. Our simulations of FAS acyl-ACP intermediates display the entrance pathway into the hydrophobic pocket of ACP in 12 out 72 trajectories. Similar to the nonsubstituted, saturated acyl chains, the intermediates undergo the same fluctuations in the solvent before entering the hydrophobic pocket (Figure 2A) (*17*). Importantly, the acyl chain intermediates are observed to enter the same hydrophobic binding pocket of ACP as the saturated acyl chains, which confirms that ACP uses the same cavity to bind these groups. Inside the hydrophobic cavity, the acyl chains explore both sub pockets I and II, which are mediated by Leu 42 and 46, consistent with what was described in our earlier MD study on saturated acyl-ACPs (*17*). This second sub pocket was subsequently experimentally verified by NMR structural studies, strongly suggesting that the conformational space sampled by the acyl chains in our simulations is consistent with their in vivo behavior (*18*, *19*). Structures of acyl-ACPs from the polyketide synthase system of *Streptomyces coelicolor* have recently been published that have covalently bound early polyketide intermediates (*18*). Although the polyketide synthase (PKS) and FAS systems are considerably different and the natural cargo can be far bulkier in the PKS system, these are the only structures available that have characterized acyl chains similar to the FAS intermediates studied here. In the PKS

structures, the C4 acyl intermediates do not enter the hydrophobic pocket, while a minor conformer of the C6 triketide is proposed to enter the cavity (*18*). The simulations also strongly support the idea that the intermediates are protected by the hydrophobic pocket of ACP, although in a different fashion from polyketide or saturated acyl chains (vide supra).

The simulations also suggest that there may be a transient point during the entry process in which the acyl chain is positioned in loop I on the surface of ACP (Figure 2C). This conformation was sampled in 28 out of 72 total trajectories that were started with a solvent-exposed acyl chain, confirming that this interaction is not an artifact of any individual simulation. In addition, a similar arrangement of the prosthetic group is seen in the NMR structure of *Plasmodium falciparium* holo-ACP, where the phosphopantetheine group is observed to interact with the same portion of loop I (*36*). In our simulations, this intermediate conformation is stabilized in two ways: First, through pronounced hydrogen bonding between the prosthetic linker and various residues in loop I, and second via a hydrophobic cushion that is formed in the groove of loop I where the acyl chain frequently lies. Such intermediates would be difficult to detect experimentally, but it might be interesting in future work to determine how loop I mutations that vary the hydrophobic character of the loop affect the kinetics of acyl chain binding and utilization by partner enzymes. Previous studies have shown that mutations in the loop I region have variable effects on ACP function, but it is difficult to draw conclusions about acyl-chain:loop I interactions based on this (*37*). As such, further experimental verification will be needed to determine the exact role of these acyl-chain:loop I interactions.

Acyl-Chain Extraction Pathway. The exact method of substrate delivery from ACP to the enzymes of the FAS system is difficult to elucidate through conventional structural techniques because this would require trapping various states along the acyl-chain delivery pathway. MD simulations are well-known to be a useful alternative technique to probe pathways between two physiologically relevant states that are readily accessible to X-ray crystallography and were therefore employed here (*38*, *39*). Our MD simulations were able to capture the extrusion of the β-ketobutyryl- and β-hydroxybutyryl-chains from ACP, which is necessary for substrate presentation to the enzymes of FA synthesis. Notably, our simulations were conducted at equilibrium with no external force applied to the simulations that would bias the outcome in any way. Each of the acyl groups that exits the hydrophobic binding cavity was four carbon groups in length, which is the shortest length examined in this study. This is not surprising, considering that bulk hydrophobic character of the acyl chains is thought to be a key stabilizing force that keeps the chain inside the pocket. This also matches the structure of the *S. coelicolor* polyketide synthase 3-oxobutyl-ACP, which was not observed to enter the hydrophobic binding pocket (*18*). In contrast to a previous study on *P. falciparum* ACP that applied steered MD to move the acyl chain out of the pocket, we did not observe a significant swinging of helix III away from helix II in our unbiased simulations (*40*). However, our butyryl derivatives are much shorter than the β-hydroxydecanoyl group studied there, which might explain these discrepancies.

We observe that the prosthetic linker is very flexible and propose that this is important for the mobility and extrusion of the entire arm, including the attached acyl chain (Figures 2B and 6). When the acyl chain is buried in the hydrophobic pocket, the prosthetic group does not rest in one well-defined position (Figure 2B). Instead, it adopts different hydrogen bonding partners as it moves between various conformations. This is important for the arm to retain its flexibility and facilitates the extrusion of the attached acyl chain. For example, if the linker only occupied one well-defined energy minimum that is separated from less favorable conformations by large energy barriers, the acyl chain would be less flexible and more difficult to extract from the protein. Instead, the phosphopantetheine group alternates between several conformations, which suggests that there are a number of linker positions of similar stability with low energy barriers, thereby ensuring that the arm remains sufficiently flexible for acyl chain delivery. This is consistent with the observation that part of the electron density of the linker group was missing in some of the acyl-ACP crystal structures (*6*, *7*). During the acyl chain extraction, the linker participates in a similar number of hydrogen bonds with the protein, independent of the acyl chain being buried in the hydrophobic binding pocket or not, which suggests there would not be a large entropic or enthalpic energy penalty upon acyl chain extraction and substrate presentation to other enzymes.

Biological Implications. ACP interacts with a large number of proteins in a variety of biological processes such as FAS, bioluminescence, and quorum sensing, among others (*9*, *11*, *12*). It is also one of the most abundant proteins in the cell, which raises the question of how specific ACPs that carry the substrate of interest are recognized (*41*). It is possible that other enzymes blindly interact with ACP and extract the carrier load without any knowledge of which substrate is bound, or alternatively, ACP could undergo slight conformational changes based on which substrate is bound in its hydrophobic core (*7*, *13*). Our proposed binding model supports a slightly altered version of this second theory (Figure 7). We propose that ACP does not undergo a large conformational change itself, but that the different acyl attachments confer slightly altered surface features that can be recognized. The β-ketone and β-hydroxyl groups are solvent-exposed in each of the trajectories such that the additional functional groups present a recognition site on ACP that may be utilized by enzymes of the FAS system. This is consistent with the fact that ACP:enzyme interactions occur primarily along helix II, the recognition helix, and loop II leading into helix III, since the hydroxyl and ketone functional groups preferentially localize in that region during the simulations (Figure 4) (*13*, *16*, *42*, *43*). In fact, in our trajectories the β-hydroxyl- and β-ketone-moieties are frequently observed to penetrate between helices II and III along with the thioester oxygen, potentially providing a recognition motif for the FAS enzymes (Figure 4B). The β-ketoacyl reductase and β-hydroxyacyl dehydratases may therefore have specific recognition sites that are dependent on the correct interaction pattern between the acyl chain intermediate and the enzyme before the substrate is extruded from ACP. This is in agreement with NMR chemical shift perturbation experiments of ACP in complex with β-ketoacyl reductase, which show that primarily residues in helices II and III are affected (*13*). This would position the partner enzyme ideally for the recognition of the β-ketone or β-hydroxyl group or for the detection of a change in helix III arrangement similar to what we observed upon acyl chain binding (Figure 3). The shortest, butyryl acyl chains that have at times been observed to exit the hydrophobic pocket spontaneously, may make the recognition process more straightforward, since the entire acyl chain is solvent exposed and there is no ambiguity in regards to the substrate that is present. The

importance of the gap between helices II and III was also proposed in a study on *P. falciparum* ACP, in which a widening was observed in concert with acyl chain binding, which is in good agreement with our observations (*19*). The hydrogen bond between the side chain of Glu47 and the amide of Ile54 (*E. coli* numbering) was observed to weaken in that study when longer acyl chains are bound (*19*). We see a similar increase in the distance between these two groups in our studies (not shown), which is related to the tips of the longer acyl chains (≥C12) penetrating into the solvent between helix II and loop II and interfering with that hydrogen bond. The two existing crystal structures of ACP:enzyme complexes provide limited information on the hypothesis that the functional group in the β position may be recognized, because neither of the enzymes involved (i.e., ACP synthase and enoyl ACP reductase) act on the β-ketoacyl or β-hydroxyacyl intermediates (*15*, *16*). Nevertheless, the interactions found in those structures primarily involve helices II and III, which is consistent with the model proposed here. According to our theory, the *trans*-2-enoyl acyl-chain intermediates do not present a specific recognition motif to the enzymes of the FAS system in our simulations and would therefore have similar properties to saturated acyl-ACP intermediates. This is supported by the observation that saturated acyl-ACPs serve as competitive inhibitors for enoyl-ACP reductases, which means that these enzymes are unable to distinguish between the *trans*-2-enoyl and saturated forms of acyl-ACP (*44*).

Understanding the molecular determinants for ACP:enzyme interactions could be invaluable for the development of novel antibacterial agents. There are already antibiotics in use that target FAS enzymes, and this area continues to be heavily investigated, not only due to the different architecture between human and bacterial systems but also due to the essential nature of the FAS (*4*, *45*, *46*). One potential approach may be to block the extrusion of acyl chains from ACP, which would disrupt a whole series of reactions since several enzymes are dependent on substrate delivery by ACP. This would make it more difficult for bacteria to develop resistance against than a mechanism that only affects one reaction. Conceivably, if essential interactions between the β-groups and the FAS enzymes can be prevented, the acyl chain would not be accessible. Similarly, modifying the interactions between the prosthetic linker and ACP might alter its flexibility and trap the acyl chain inside the hydrophobic pocket. Working toward that goal, structural and biophysical data on the conformations of ACP, as induced by the binding to acyl chain elongation intermediates, will be needed to further verify the first observations made here.

ACKNOWLEDGMENT

The authors would like to thank Eoin Coll for helpful discussions about the MD simulations and analysis.

SUPPORTING INFORMATION AVAILABLE

Detailed simulation procedures and tables providing a qualitative overview of the results of each trajectory. In addition, the results of a suite of test simulations performed on β-hydroxydecanoyl-ACP are provided that were conducted with either a shorter time step (2 fs), a newer version of the GROMOS96 forcefield (*29*), or slightly altered charges based on PRODRG (*30*). This material is available free of charge via the Internet at http://pubs.acs.org.

REFERENCES

1. White, S. W., Zheng, J., Zhang, Y. M., and Rock, C. O. (2005) The structural biology of type II fatty acid biosynthesis. *Annu. Rev. Biochem. 74*, 791–831.
2. Lu, Y. J., Zhang, Y. M., and Rock, C. O. (2004) Product diversity and regulation of type II fatty acid synthases. *Biochem. Cell Biol. 82*, 145–155.
3. Zhang, Y. M., and Rock, C. O. (2008) Membrane lipid homeostasis in bacteria. *Nat. Rev. Microbiol. 6*, 222–233.
4. Wright, H. T., and Reynolds, K. A. (2007) Antibacterial targets in fatty acid biosynthesis. *Curr. Opin. Microbiol. 10*, 447–453.
5. Byers, D. M., and Gong, H. (2007) Acyl carrier protein: structure-function relationships in a conserved multifunctional protein family. *Biochem. Cell Biol. 85*, 649–662.
6. Roujeinikova, A., Baldock, C., Simon, W. J., Gilroy, J., Baker, P. J., Stuitje, A. R., Rice, D. W., Slabas, A. R., and Rafferty, J. B. (2002) X-ray crystallographic studies on butyryl-ACP reveal flexibility of the structure around a putative acyl chain binding site. *Structure 10*, 825–835.
7. Roujeinikova, A., Simon, W. J., Gilroy, J., Rice, D. W., Rafferty, J. B., and Slabas, A. R. (2007) Structural studies of fatty acyl-(acyl carrier protein) thioesters reveal a hydrophobic binding cavity that can expand to fit longer substrates. *J. Mol. Biol. 365*, 135–145.
8. Zornetzer, G. A., Fox, B. G., and Markley, J. L. (2006) Solution structures of spinach acyl carrier protein with decanoate and stearate. *Biochemistry 45*, 5217–5227.
9. Byers, D. M., and Meighen, E. A. (1985) Acyl-acyl carrier protein as a source of fatty acids for bacterial bioluminescence. *Proc. Natl. Acad. Sci. U. S. A. 82*, 6085–6089.
10. Anderson, M. S., and Raetz, C. R. (1987) Biosynthesis of lipid A precursors in Escherichia coli. A cytoplasmic acyltransferase that converts UDP-*N*-acetylglucosamine to UDP-3-*O*-(*R*-3-hydroxymyristoyl)-*N*-acetylglucosamine. *J. Biol. Chem. 262*, 5159–5169.
11. Schaefer, A. L., Val, D. L., Hanzelka, B. L., Cronan, J. E., Jr., and Greenberg, E. P. (1996) Generation of cell-to-cell signals in quorum sensing: acyl homoserine lactone synthase activity of a purified *Vibrio fischeri* LuxI protein. *Proc. Natl. Acad. Sci. U. S. A. 93*, 9505–9509.
12. Butland, G., Peregrín-Alvarez, J. M., Li, J., Yang, W. H., Yang, X. C., Canadien, V., Starostine, A., Richards, D., Beattie, B., Krogan, N., Davey, M., Parkinson, J., Greenblatt, J., and Emili, A. (2005) Interaction network containing conserved and essential protein complexes in *Escherichia coli*. *Nature 433*, 531–537.
13. Zhang, Y. M., Wu, B., Zheng, J., and Rock, C. O. (2003) Key residues responsible for acyl carrier protein and beta-ketoacyl-acyl carrier protein reductase (FabG) interaction. *J. Biol. Chem. 278*, 52935–52943.
14. Holak, T. A., Kearsley, S. K., Kim, Y., and Prestegard, J. H. (1988) Three-dimensional structure of acyl carrier protein determined by NMR pseudoenergy and distance geometry calculations. *Biochemistry 27*, 6135–6142.
15. Parris, K. D., Lin, L., Tam, A., Mathew, R., Hixon, J., Stahl, M., Fritz, C. C., Seehra, J., and Somers, W. S. (2000) Crystal structures of substrate binding to *Bacillus subtilis* holo-(acyl carrier protein) synthase reveal a novel trimeric arrangement of molecules resulting in three active sites. *Structure 8*, 883–895.
16. Rafi, S., Novichenok, P., Kolappan, S., Zhang, X. J., Stratton, C. F., Rawat, R., Kisker, C., Simmerling, C., and Tonge, P. J. (2006) Structure of acyl carrier protein bound to FabI, the FASII enoyl reductase from *Escherichia coli*. *J. Biol. Chem. 281*, 39285–39293.
17. Chan, D. I., Stockner, T., Tieleman, D. P., and Vogel, H. J. (2008) Molecular Dynamics simulations of the apo-, holo-, and acyl-forms of *Escherichia coli* acyl carrier protein. *J. Biol. Chem. 283*, 33620–33629.
18. Evans, S. E., Williams, C., Arthur, C. J., Ploskon, E., Wattana-Amorn, P., Cox, R. J., Crosby, J., Willis, C. L., Simpson, T. J., and Crump, M. P. (2009) Probing the interactions of early polyketide intermediates with the actinorhodin ACP from *S. coelicolor* A3(2). *J. Mol. Biol. 389*, 511–528.
19. Upadhyay, S. K., Misra, A., Srivastava, R., Surolia, N., Surolia, A., and Sundd, M. (2009) Structural insights into the acyl intermediates of the *Plasmodium falciparum* fatty acid synthesis pathway. *J. Biol. Chem. 284*, 22390–22400.
20. Scott, W. R. P., Hunenberger, P. H., Tironi, I. G., Mark, A. E., Billeter, S. R., Fennen, J., Torda, A. E., Huber, T., Kruger, P., and van Gunsteren, W. F. (1999) The GROMOS biomolecular simulation program package. *J. Phys. Chem. B 103*, 3596–3607.
21. Bachar, M., Brunelle, P., Tieleman, D. P., and Rauk, A. (2004) Molecular dynamics simulation of a polyunsaturated lipid bilayer susceptible to lipid peroxidation. *J. Phys. Chem. B 108*, 7170–7179.

22. Antes, I., Thiel, W., and van Gunsteren, W. F. (2002) Molecular dynamics simulations of photoactive yellow protein (PYP) in three states of its photocycle: a comparison with X-ray and NMR data and analysis of the effects of Glu46 deprotonation and mutation. *Eur. Biophys. J. 31*, 504–520.
23. Chandrasekhar, I., Kastenholz, M., Lins, R. D., Oostenbrink, C., Schuler, L. D., Tieleman, D. P., and van Gunsteren, W. F. (2003) A consistent potential energy parameter set for lipids: dipalmitoylphosphatidylcholine as a benchmark of the GROMOS96 45A3 force field. *Eur. Biophys. J. 32*, 67–77.
24. Berendsen, H. J. C., van der Spoel, D., and van Drunen, R. (1995) Gromacs - A message-passing parallel Molecular-Dynamics implementation. *Comput. Phys. Commun. 91*, 43–56.
25. Lindahl, E., Hess, B., and van der Spoel, D. (2001) GROMACS 3.0: a package for molecular simulation and trajectory analysis. *J. Mol. Model 7*, 306–317.
26. Feenstra, K. A., Hess, B., and Berendsen, H. J. C. (1999) Improving efficiency of large time-scale molecular dynamics simulations of hydrogen-rich systems. *J. Comput. Chem. 20*, 786–798.
27. van der Spoel, D., and Lindahl, E. (2003) Brute-force molecular dynamics simulations of Villin headpiece: Comparison with NMR parameters. *J. Phys. Chem. B 107*, 11178–11187.
28. Humphrey, W., Dalke, A., and Schulten, K. (1996) VMD: visual molecular dynamics. *J. Mol. Graph 14*, 33–38.
29. Oostenbrink, C., Soares, T. A., van der Vegt, N. F. A., and van Gunsteren, W. F. (2005) Validation of the 53A6 GROMOS force field. *Eur. Biophys. J. Biophys. 34*, 273–284.
30. Schüttelkopf, A. W., and van Aalten, D. M. F. (2004) PRODRG: a tool for high-throughput crystallography of protein-ligand complexes. *Acta Crystallogr. D Biol. Crystallogr. 60*, 1355–1363.
31. Wu, B. N., Zhang, Y. M., Rock, C. O., and Zheng, J. J. (2009) Structural modification of acyl carrier protein by butyryl group. *Protein Sci. 18*, 240–246.
32. Rock, C. O., and Jackowski, S. (2002) Forty years of bacterial fatty acid synthesis. *Biochem. Biophys. Res. Commun. 292*, 1155–1166.
33. Maier, T., Leibundgut, M., and Ban, N. (2008) The crystal structure of a mammalian fatty acid synthase. *Science 321*, 1315–1322.
34. Ploskon, E., Arthur, C. J., Evans, S. E., Williams, C., Crosby, J., Simpson, T. J., and Crump, M. P. (2008) A mammalian type I fatty acid synthase acyl carrier protein domain does not sequester acyl chains. *J. Biol. Chem. 283*, 518–528.
35. Brignole, E. J., Smith, S., and Asturias, F. J. (2009) Conformational flexibility of metazoan fatty acid synthase enables catalysis. *Nat. Struct. Mol. Biol. 16*, 190–197.
36. Sharma, A. K., Sharma, S. K., Surolia, A., Surolia, N., and Sarma, S. P. (2006) Solution structures of conformationally equilibrium forms of holo-acyl carrier protein (PfACP) from *Plasmodium falciparum* provides insight into the mechanism of activation of ACPs. *Biochemistry 45*, 6904–6916.
37. Worsham, L. M., Earls, L., Jolly, C., Langston, K. G., Trent, M. S., and Ernst-Fonberg, M. L. (2003) Amino acid residues of *Escherichia coli* acyl carrier protein involved in heterologous protein interactions. *Biochemistry 42*, 167–176.
38. Karplus, M., and Kuriyan, J. (2005) Molecular dynamics and protein function. *Proc. Natl. Acad. Sci. U. S. A. 102*, 6679–6685.
39. Stockner, T., Vogel, H. J., and Tieleman, D. P. (2005) A salt-bridge motif involved in ligand binding and large-scale domain motions of the maltose-binding protein. *Biophys. J. 89*, 3362–3371.
40. Colizzi, F., Recanatini, M., and Cavalli, A. (2008) Mechanical features of *Plasmodium falciparum* acyl carrier protein in the delivery of substrates. *J. Chem. Inf. Model. 48*, 2289–2293.
41. Rock, C. O., and Jackowski, S. (1982) Regulation of phospholipid synthesis in *Escherichia coli*. Composition of the acyl-acyl carrier protein pool in vivo. *J. Biol. Chem. 257*, 10759–10765.
42. Zhang, Y. M., Marrakchi, H., White, S. W., and Rock, C. O. (2003) The application of computational methods to explore the diversity and structure of bacterial fatty acid synthase. *J. Lipid Res. 44*, 1–10.
43. Gong, H. S., Murphy, A., McMaster, C. R., and Byers, D. M. (2007) Neutralization of acidic residues in helix II stabilizes the folded conformation of acyl carrier protein and variably alters its function with different enzymes. *J. Biol. Chem. 282*, 4494–4503.
44. Heath, R. J., and Rock, C. O. (1996) Regulation of fatty acid elongation and initiation by acyl-acyl carrier protein in *Escherichia coli*. *J. Biol. Chem. 271*, 1833–1836.
45. Zhang, Y. M., White, S. W., and Rock, C. O. (2006) Inhibiting bacterial fatty acid synthesis. *J. Biol. Chem. 281*, 17541–17544.
46. Lee, J. Y., Jeong, K. W., Lee, J. U., Kang, D. I., and Kim, Y. (2009) Novel *E. coli* beta-ketoacyl-acyl carrier protein synthase III inhibitors as targeted antibiotics. *Bioorg. Med. Chem. 17*, 1506–1513.